A 2D Array of Copper(I) Catenane Catalyst Grafted on a Metal-Organic Layer for High Fidelity Cross-Coupling

Yi-Xiang Shi,[1†] Lihui Zhu,[1,2,†] Yulin Deng,[1] Xiaoyong Mo,[1] Yufeng Wang,[1] Edmund C. M. Tse,[1] Ho Yu Au-Yeung[1,2,3,*]

[1]Department of Chemistry, The University of Hong Kong, Pokfulam Road, Hong Kong, PR China

[2]State Key Laboratory of Synthetic Chemistry, University of Hong Kong, Pokfulam Road, Hong Kong, PR China

[3]CAS-HKU Joint Laboratory on New Materials, The University of Hong Kong, Pokfulam Road, Hong Kong, PR China

[†]These authors contribute equally

[*]Corresponding author

Abstract

While Earth abundant metals are green and sustainable alternatives to precious metals for catalytic chemical conversions, the fast ligand exchange involving most of these metals renders their development into robust, reusable catalysts very challenging. Described in this work is a new type of heterogeneous catalyst derived from a 2D metal-organic layer (MOL) grafted with catenane-coordinated Cu(I) complexes. In addition to the good substrate accessibility, easy functionalization and other favorable features due to the MOL support, the anchored catenane ligands also provide a well-defined coordination environment and good kinetic stability to the coordinated Cu(I). Catalytic studies using phenols and bromodicarbonyls as the substrates showed that the Cu(I) catenane-grafted MOL resulted in the exclusive C–O coupling of the substrates, whereas a control catalyst in which the catenanes are replaced by non-interlocked macrocyclic ligands was found to lead to also a C–C coupling due to the uncontrolled formation of oxidized copper active site. The integration of mechanically interlocked catalyst to extended framework support thus represent an unexplored potential of exploiting labile, Earth-abundant metals for sustainable catalysis under challenging conditions.

Introduction

Metal–organic frameworks (MOFs), consisting of organic linkers and metal ions/clusters, are an emerging class of hybrid porous crystalline materials for developing site-isolated heterogeneous metal catalysts.[1–7] In addition to the long-range crystalline order, high stability and tunable connectivity,[8,9] two-dimensional metal–organic layers (MOLs) are particularly attractive for catalyst development because their layered structures are readily accessible for incorporating metal active sites, as well as facilitating substrate diffusion that enhances the overall catalytic efficiency.[10–14] While anchoring of metal ions or complexes onto a formed framework is one most straightforward method to obtain MOF/MOL-based catalysts,[15,16] the facile ligand exchange involving most earth abundant metals not only could lead to the formation of multiple active sites, but also result in the interactions and loss of the metal active sites that will compromise the catalyst activity, selectivity, stability and recyclability.[17–20] New designs of MOFs/MOLs that contain robust, isolated and coordinatively well-defined active sites are therefore necessary for developing new heterogenous catalysts derived from base metals for sustainable catalysis.[21–24]

In this regard, mechanical interlocking of coordination ligands offers a unique opportunity for obtaining metal catalysts with a dynamic yet highly stable coordination.[25–31] Due to the interlocking, complete ligand dissociation is prohibited.[32,33] Hence, non-specific interactions at the metal active sites are minimized, and a kinetically stabilized, well-defined coordination can be maintained throughout the catalysis as well as the catalyst recycling procedures.[34–36] Other characteristics due to mechanical bond such as dynamic co-conformational changes and effects from mechanical confinement can also be engineered into favorable catalysis features such as new selectivity, longer lifetime and sustained activity.[37,38] Employing mechanically interlocked ligands such as catenane is therefore a promising direction to overcome challenges in integrating earth abundant metal catalysts into MOFs/MOLs.[39,40]

As a proof-of-concept, we describe in this work the development of an active MOL grafted with a 2D array of isolated, catenane-coordinated Cu(I) catalytic sites via simple linker replacement and click functionalization. Model catalytic studies using the new MOL as a heterogeneous catalyst for the cross-dehydrogenative C–O coupling of phenols and bromodicarbonyls showed that the C–O coupled product was formed exclusively in good yield and efficiency with a good recyclability. Control reactions using an analogous MOL grafted with a non-interlocked Cu(I) complex was found to also result in a ketomalonate via a C–C coupling mediated by residual Cu(II), showing that the kinetically stabilized catenane-supported Cu(I) is advantageous and critical to the high-fidelity catalysis of the MOL-based catalyst (Scheme 1).

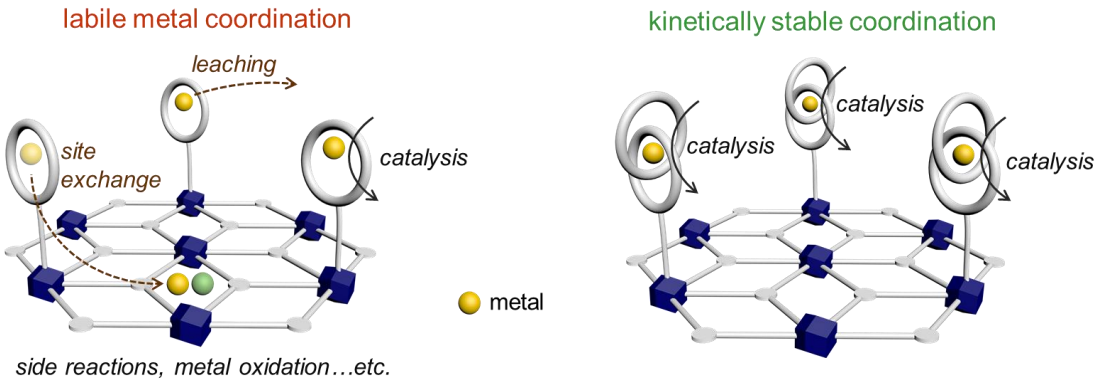

Scheme 1. Comparison of MOL-derived heterogenous catalyst with metal active sites supported by conventional and interlocked ligands.

Results and Discussion

Design, Synthesis and Characterization. A known MOL derived from 4,4′,4″-benzene-1,3,5-triyl-tris(benzoate) (BTB) and $Zr_6(\mu_3\text{-}O)_4(\mu_3\text{-}OH)_4(H_2O)_4(OH)_4$ clusters (i.e. Zr-BTB) with a Kagome dual (*kgd*) topology was chosen as the support platform for catalyst grafting because of its exceptional stability, accessibility and ease in ligand replacement for hierarchical integration of extraneous active sites.[41,42] Ultrathin Zr-BTB nanosheets were synthesized following a literature procedure.[43] The vertically capped benzoates at the 6-connecting $[Zr_6(\mu_3\text{-}O)_4(\mu_3\text{-}OH)_4]$ clusters were substituted by six pairs of OH^-/H_2O ligands upon treatment with HCl/H_2O, and subsequently replaced by the stronger coordinating 3-azidopropionate to install clickable azide handles to give Zr-BTB-Az.[44] For the metal catenane complex to be grafted onto the MOL, the alkyne-functionalized [Cu**C**]PF_6 was selected as similar Cu(I) catenane complexes have been previously demonstrated as active catalyst towards cross-coupling reactions and electrochemical reduction.[29–32] The functionalized MOL, Zr-BTB-[Cu**C**], with a 2D array of the Cu(I) catenanes on the MOL was obtained by copper-catalyzed azide-alkyne click reaction, followed by extensive solvent washing to remove the copper catalyst for the click reaction (Figure 1). Due to the good kinetic stability from catenand effect, the Cu(I) catenane complex was found to remain intact after the grafting and extensive washing, highlighting the easy synthesis of the catenane-grafted MOL without the need of metal reintroduction. Compared with the direct construction of MOLs using catenane complexes as the organic linkers, the present grafting method is straightforward and reliable, and the crystallinity and structural integrity of the MOLs will not be influenced by the relatively large size and flexibility of the catenanes.

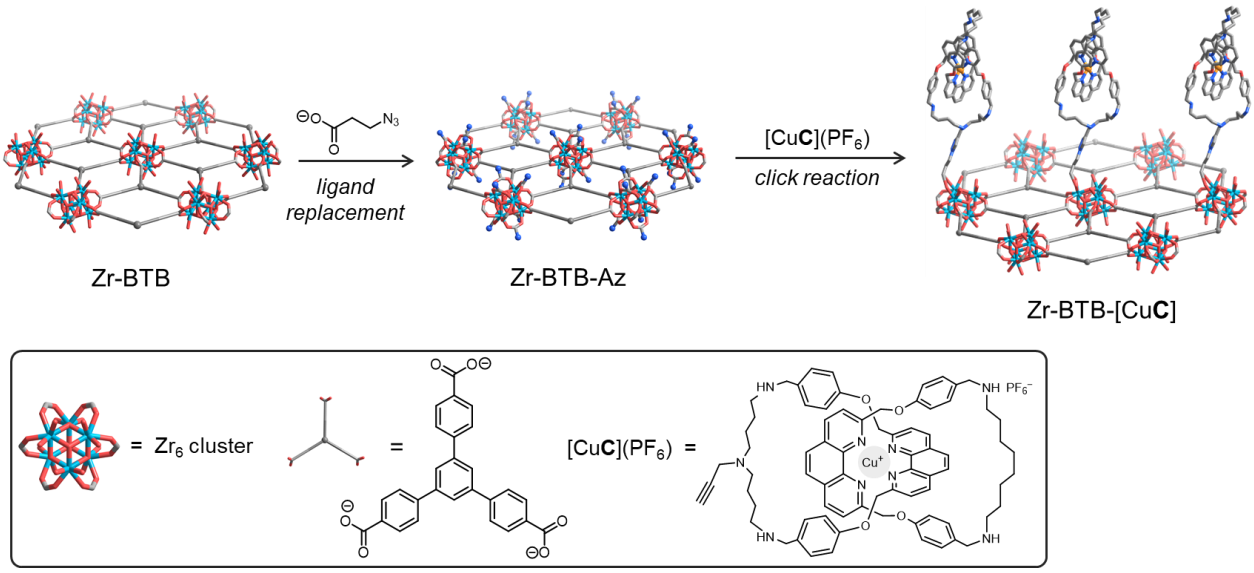

Figure 1. Synthesis of Zr-BTB-[Cu**C**] by grafting.

Fourier-transform infrared (FT-IR) spectrum of the obtained Zr-BTB-[Cu**C**] showed an azide stretching band at 2096 cm^{-1} of only very weak intensity as compared to that obtained before the click reaction, and the presence of C–N (1237 cm^{-1}), C–H (2905 cm^{-1} and 2984 cm^{-1}) and N–H (3665 cm^{-1}) stretching bands of the Cu(I) catenane are consistent with the successful grafting of the catenane onto the MOLs (Figure S14).[45] Energy-dispersive spectroscopic (EDS) elemental mapping showed a uniform Cu distribution on the surface of the Zr-BTB-[Cu**C**] monolayer (Figure 2b), and a loading of two copper (as catenane complexes) per three Zr_6 clusters was found based on EDS and inductively coupled plasma mass spectrometry (ICP–MS) (Table S1). Solid-state UV–vis spectrum of Zr-BTB-[Cu**C**] shows a broad absorbance in the visible region from 300 nm to 700 nm, with an absorption edge that is more red-shifted than that of the pristine Zr-BTB (Figure S15). The X-ray photoelectron spectroscopy (XPS) measurements showed the presence of C, O, N, F, Cu and Zr elements in the as-prepared Zr-BTB-[Cu**C**] samples (Figures 2 and S16–S19). The high-resolution Cu *2p* XPS spectra of both [Cu**C**]PF_6 and the Zr-BTB-[Cu**C**] show the Cu^+/Cu^0 states with their respective $2p_{3/2}$ and $2p_{1/2}$ peaks at 932.2 eV and 952.1 eV (Figure 2d). The XPS spectrum of the Zr-BTB-[Cu**C**] revealed a slight shift of the Zr 3*d* region towards a lower binding energy (~0.31 eV) when compared to that of the pure Zr-BTB phase (Figure S20), which could be explained by a redistribution of the electrons causing a strain, and/or restructuring of the Zr-BTB surface due to interactions with the anchored Cu(I) catenanes.[46]

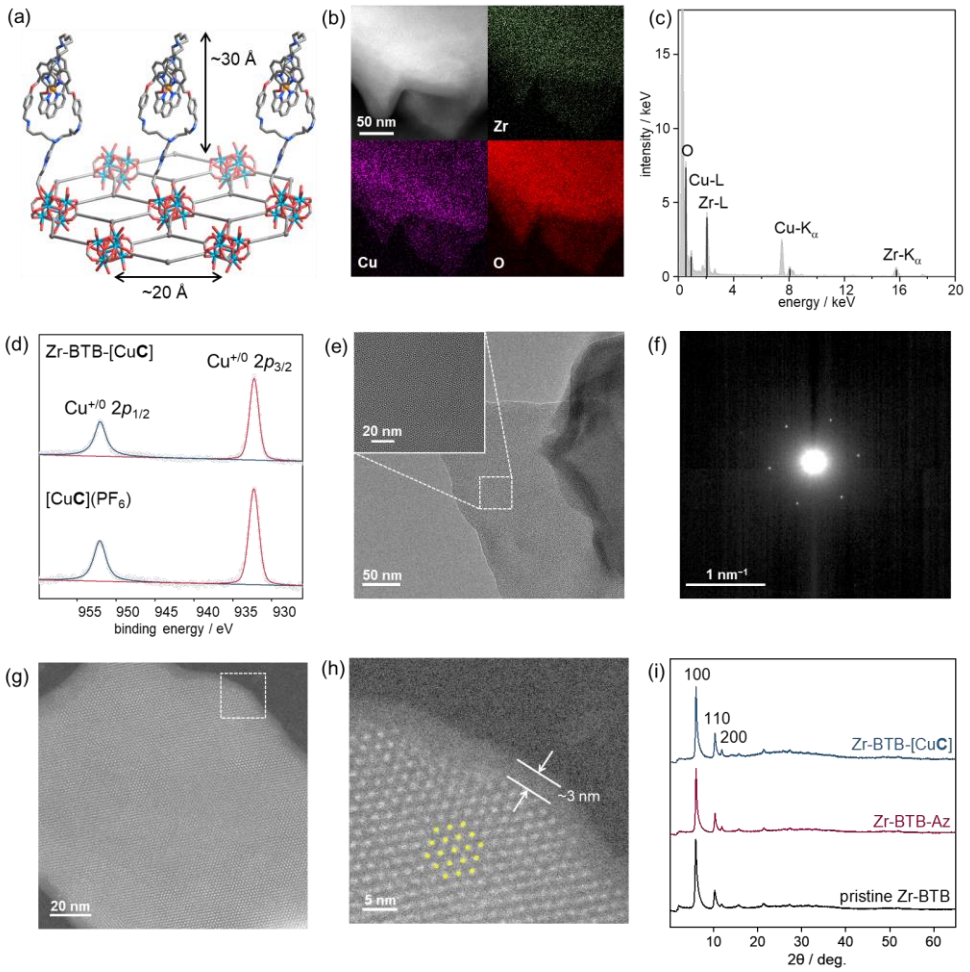

Figure 2. (a) Model of Zr-BTB-[Cu**C**] (C, grey; O, red; N, blue; Zr, cyan; Cu, orange; H atoms and PF_6^- ions are omitted for clarity); (b) HAADF image and EDS elemental mappings of Zr-BTB-[Cu**C**]; (c) EDX spectrum of Zr-BTB-[Cu**C**]; (d) high-resolution Cu 2*p* XPS spectra of Zr-BTB-[Cu**C**] (top) and [Cu**C**](PF_6) (bottom); (e) HR-TEM images of Zr-BTB-[Cu**C**] (inset: enlarged view of the selected area); (f) SAED pattern showing a hexagonal symmetry with a measured interplanar spacing of 17.4 Å (g) high-resolution STEM-HAADF image of the interface of Zr-BTB-[Cu**C**]; (h) enlarged view of the selected region of the STEM-HAADF image in (g) showing a hexagonal arrangement of the Zr_6 cluster (yellow dots) and an amorphous layer of ~3 nm at the edge of the MOLs; (i) powder X-ray diffraction patterns of the obtained Zr-BTB-[Cu**C**] (top), Zr-BTB-Az before click functionalization (middle) and the parent monolayered Zr-BTB (bottom).

Morphology and structure of Zr-BTB-[Cu**C**] were further characterized by transmission electron microscopy (TEM) and aberration-corrected high-angle annular dark-field scanning transmission electron microscopy (HAADF-STEM) (Figures 2 and S21–S23). A wrinkled monolayer morphology was found in the TEM images of Zr-BTB-[Cu**C**] (Figures 2e).[47] High resolution TEM (HR-TEM) and HAADF images revealed hexagonal lattice fringes expected for a 2D 3,6-connected *kgd* network, with a distance of ~2.1 nm between adjacent spots that represent the Zr_6 clusters (Figures 2g and S23). Notably, an amorphous layer of thickness ~3 nm was also observed at the edge of the nanosheet (Figure 2h), consistent to the

surface of the MOLs being decorated by the Cu(I) catenanes. The selected area electron diffraction pattern (SAED) also confirms the hexagonal symmetry along the *c* axis perpendicular to the 2D layer with a measured spacing of ~17.4 Å between the crystal planes, which are consistent to the reported *kgd* lattice of a related Zr-MOL with a hexagonal unit cell (*a* = 19.4 Å) (Figure 2f). The powder X-ray diffraction (PXRD) patterns obtained for Zr-BTB-[Cu**C**] showed that structural integrity of the nanosheets is retained after the grafting, and that Zr-BTB-[Cu**C**] is structurally highly similar to the parent Zr-BTB (Figure 2i). On the other hand, N_2 sorption measurements showed a lower Brunauer–Emmett–Teller (BET) surface areas of 410 m^2/g for Zr-BTB-[Cu**C**]$^+$ when compared to that of the parent Zr-BTB (527 m^2/g), which could be ascribed to the partial blocking of the adsorption surface by the Cu(I) catenane at the nodes (Figure S24). Overall, all the characterization data are consistently showing that the Cu(I) catenane has been successfully grafted onto the surface of the Zr-BTB nanosheets, and the original crystalline phase is remained unaffected by the post-modification.

A related MOL in which the Cu(I) catenane was replaced by the non-interlocked Cu(I) macrocyclic complex [Cu**M**](PF_6) was also prepared as a control for studying the effect of ligand interlocking in the catalysis. With only the non-interlocked phenanthroline, Cu(I) coordination to **M** is less strong, and hence the free macrocycle **M** was used for grafting onto Zr-BTB by click reaction. The residual copper was removed by washing with aqueous EDTA, and [$Cu(MeCN)_4$](PF_6) was re-introduced to give Zr-BTB-[Cu**M**] (Figure S25). A homogeneous Cu distribution was observed by EDS elemental mapping on the obtained Zr-BTB-[Cu**M**] (Figure S26), and a PXRD pattern similar to that of the parent Zr-BTB was found, showing that structural integrity of the nanosheets is retained after the post-synthetic grafting (Figure S27).

Evaluation of Catalytic Performance. With the successful synthesis of Zr-BTB-[Cu**C**], its catalytic performance as a heterogenous catalyst was tested using the C–O coupling of phenols and bromodicarbonyls as a model reaction.[48,49] Previously, related molecular Cu(I) catenane complexes have been demonstrated as effective catalyst for the same coupling reaction, and the mechanical bond in the catenane ligand has been shown to be advantageous for enhancing the catalyst activity and stability.[32] As shown in Table 1, by using 2 mol% (per Cu) of Zr-BTB-[Cu**C**], coupling of phenol **1** and diethylbromomalonate **2** in the presence of 2 eq. K_2CO_3 at 20 °C gave **3** in 77% yield. Increasing the catalyst loading to 5 mol% or the reaction temperature to 50 °C gave a higher yield of **3** at 91% and 90% (with 87% isolated yield) respectively. On the other hand, performing the coupling at 50 °C with only 0.1 mol% of the catalyst did not compromise catalysis efficiency significantly, and **3** was obtained in 75% yield. Control experiment using 2 mol% of the non-functionalized Zr-BTB resulted in no coupling product, showing that the specific Cu(I) catenane coordination is essential to the good catalytic efficiency of Zr-BTB-[Cu**C**].[50,51] Indeed, when the control catalyst Zr-BTB-[Cu**M**] (2 mol%, per Cu) that also features a phenanthroline coordination was tested, **3** was only obtained in 33% yield after a 24-hour reaction at 20 °C, and the ketomalonate **4**, probably due to a C–C coupling, was also unexpectedly obtained as a side-product in 9% yield. Different than the case of Zr-BTB-[Cu**C**], repeating the coupling reaction mediated by Zr-BTB-[Cu**M**] at 50 °C has no obvious effect on the C–O coupling efficiency and **3** was formed in 35%, but instead promoted the C–C coupling with **4** obtained in 36% yield.

Table 1. Catalysis on dehydrogenative C–O cross-coupling.

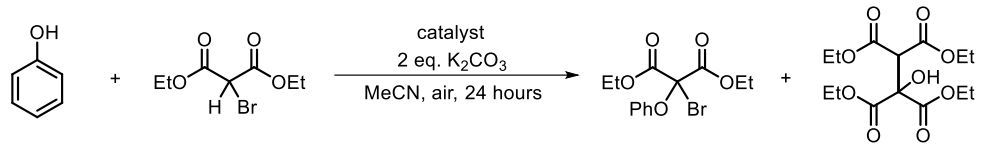

1 **2** **3** **4**

entry	catalyst	temp.	yield of **3**	yield of **4**
1	2 mol% Zr-BTB-[Cu**C**]	20 °C	77%	n.d.
2	5 mol% Zr-BTB-[Cu**C**]	20 °C	91%	n.d.
3	2 mol% Zr-BTB-[Cu**C**]	50 °C	90%[a]	n.d.
4	0.1 mol% Zr-BTB-[Cu**C**]	50 °C	75%	n.d.
5	2 mol% Zr-BTB	20 °C	n.d.	n.d.
6	2 mol% Zr-BTB-[Cu**M**]	20 °C	33%	9%
7	2 mol% Zr-BTB-[Cu**M**]	50 °C	35%	36%
8[b]	2 mol% Zr-BTB-[Cu**M**]	20 °C	51%	n.d.
9	2 mol% Zr-BTB-[Cu**C**] + 20 mol% $Cu(BF_4)_2$	50 °C	50%	50%

Reaction was conducted with **1a** (0.1 mmol) and **2a** (0.22 mmol) in 0.5 mL MeCN for 24 hours. Yield determined by ^{1}H NMR using 1,3,5-trimethoxybenzene as internal standard. [a] Isolated yield = 87%. [b] Reaction was performed under argon.

Formation of **4** is enigmatic and the C–C coupling was not observed when Cu(I) catenanes were used as the catalyst in both heterogeneous and homogeneous conditions. A study by Miao, Sun and co-workers have proposed that **4** could be formed from ketomalonate **2′′′′**, which in turn could be obtained from a reaction between the α-malonate radical **2′′** and molecular oxygen, followed by a subsequent Cu(II)-mediated cleavage of the resulting peroxy radical **2′′′**.[52] Indeed, performing the coupling using Zr-BTB-[Cu**M**] under argon at 50 °C resulted in no formation of **4** and the yield of **3** increased to 51%, not only supporting that molecular oxygen are essential, but also hinting at the presence of a Cu(II) species in the case of Zr-BTB-[Cu**M**]. Nevertheless, **4** could be formed in 50% yield by performing the catalysis using 2 mol% of Zr-BTB-[Cu**C**] at 50 °C under air with the presence of 20 mol% of $Cu(BF_4)_2$, reinforcing that the C–C coupling is due to the presence of Cu(II) (Scheme 2). High-resolution Cu 2*p* XPS spectra of Zr-BTB-[Cu**M**] recovered from the catalysis mixture indeed showed the presence of Cu^{2+} with the $2p_{3/2}$ and $2p_{1/2}$ peaks at 934.5 eV and 954.2 eV (Figure 3a), and these peaks are not observed in the corresponding spectra of the recovered Zr-BTB-[Cu**C**], hence highlighting the critical roles of the catenane ligand in maintaining the Cu(I) resting state in the high-fidelity C–O cross-coupling. As a result, mechanical interlocking of the ligand, on one hand, can restrict changes of the coordination geometry and stabilize the Cu(I) from air oxidation (i.e. the catenand effect), and on the other hand, also inhibits the metal from scrambling to other potential coordination sites within the MOLs (e.g. the triazoles), and as such a well-defined coordination environment with predictable activity can be maintained throughout the different stages of the catalysis.

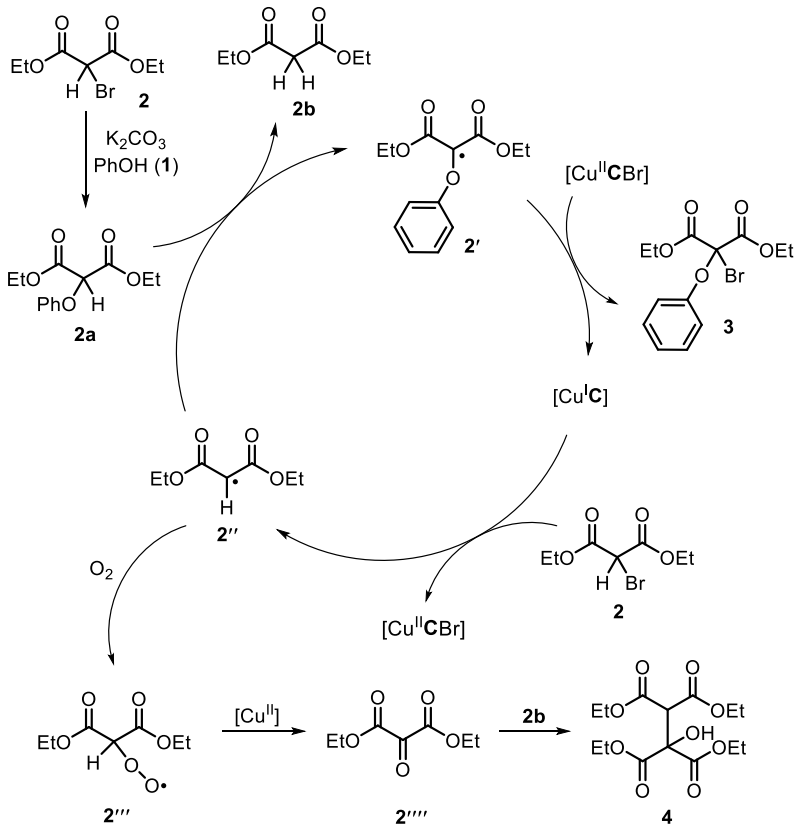

Scheme 2. Proposed mechanism for the C–O and C–C coupling.

Robustness of Zr-BTB-[Cu**C**] as a heterogenous catalyst was then evaluated by recycling experiments. Each round of reaction was conducted with 3 mmol of phenol **1** (30 times of that used in the condition screening), with 2.2 eq. of **2** and 2 mol% of Zr-BTB-[Cu**C**] in 15 mL MeCN at 50 ℃ in air for 24 hours. After the reaction, Zr-BTB-[Cu**C**] was separated from the reaction mixture by centrifugation and simple acetonitrile/water washing, and then directly used in the next round of catalysis without further treatment or activation. A good catalytic activity was maintained with the C–O coupled product **3** consistently obtained in 85%–83% yields in five consecutive rounds of reaction (Figure S28). PXRD and SEM characterization of the recovered Zr-BTB-[Cu**C**] after the last round of reaction also showed no observable difference in the crystallinity and morphology as compared to that of the pristine sample, demonstrating a good robustness of the MOL-based catenane catalyst (Figure 3). Finally, a good substrate scope was also found for Zr-BTB-[Cu**C**], and phenols with substituents of various electronic and steric properties can be efficiently coupled to give the corresponding coupling products in 83% to 95% yields (Table 2).

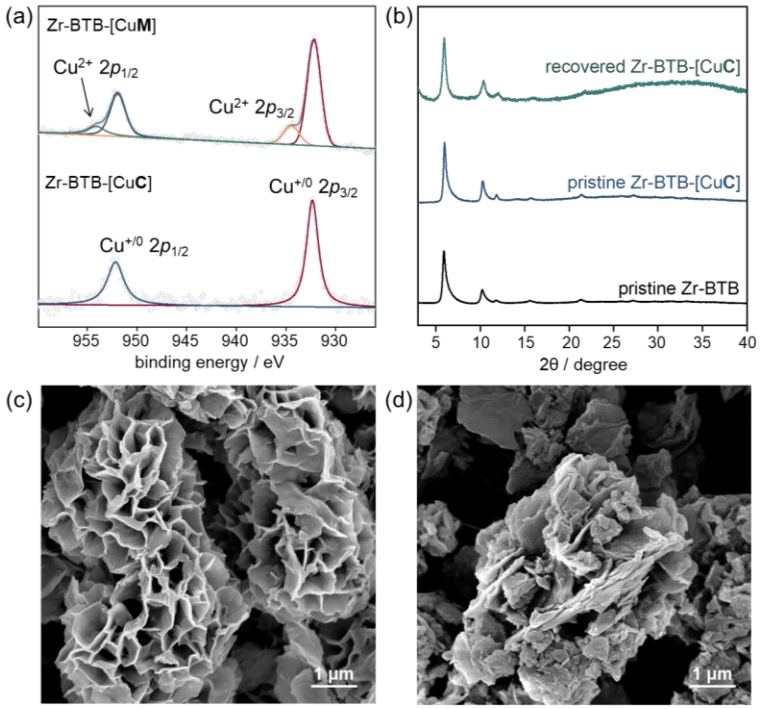

Figure 3. (a) XPS spectra of Zr-BTB-[Cu**M**] (top) and Zr-BTB-[Cu**C**] recovered after catalysis; (b) PXRD patterns of recovered (top) and pristine (middle) sample of Zr-BTB-[Cu**C**], and that of pristine Zr-BTB; and SEM images of (c) a pristine sample and (d) a recovered sample of Zr-BTB-[Cu**C**] after catalysis.

Table 2. Substrate scope of the C–O coupling catalyzed by Zr-BTB-[Cu**C**]

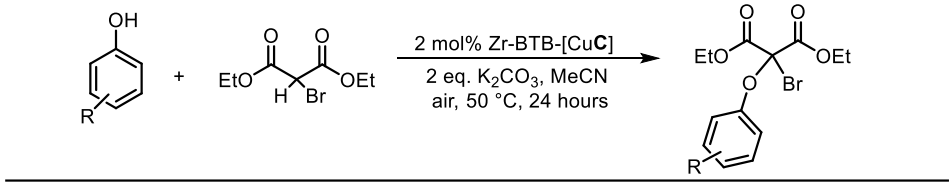

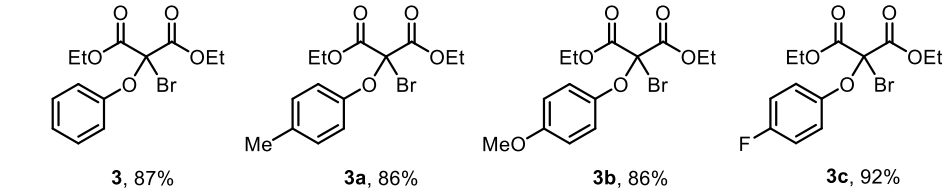

3, 87% **3a**, 86% **3b**, 86% **3c**, 92%

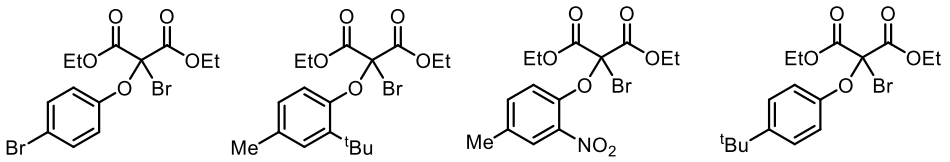

3d, 95% **3e**, 84% **3f**, 87% **3g**, 83%

Reactions were performed with the corresponding phenol (0.1 mmol), diethyl bromomalonate (0.22 mmol), Zr-BTB-[Cu**C**] (0.002 mmol) and K_2CO_3 (0.2 mmol) in 0.5 mL MeCN at 50 °C in air for 24 hours. Reported are isolated yields.

Conclusion

In summary, by advantageously employing the stable yet dynamic coordination provided by catenane ligands, a catalytically active MOL containing isolated Cu(I) active sites has been successfully developed by a straightforward post-synthetic grafting method. The kinetically stabilized Cu(I) catenanes not only can withstand the various conditions in the synthesis and recycling to give a robust catalyst, but also provide a coordinatively well-defined structure for the Cu(I) that is essential for the catalyst selectivity and activity. The Zr-BTB-[Cu**C**] catalyst is active towards the dehydrogenative cross-coupling of phenols and bromodicarbonyls, with a good activity to give the C–O coupled product in high yields (~90%), good substrate scope and good recyclability. Control experiments using a similar MOL grafted with a non-interlocked Cu(I) complex showed that a C–C coupled product, mediated by a Cu(II), can also be formed as a side-product, indicating the crucial role of the catenane ligand in maintaining the specific Cu(I) coordination for the high-fidelity C–O coupling. This proof-of-concept study hence demonstrates the synergy and potential from combining MOLs and mechanically interlocked molecules for developing new catalytic systems, particularly those derived from earth abundant metals with facile ligand exchange, with favorable features from the two unique classes of chemical entity.

Acknowledgement

This work is supported by a General Research Fund (17313222) and a Collaborative Research Fund (C7075-21G) from the Research Grants Councils of Hong Kong. Y. D. is a recipient of a Postgraduate Scholarship from HKU. We acknowledge UGC funding administered by HKU for support of the Electrospray Ionisation Quadrupole Time-of-Flight Mass Spectrometry Facilities under the support for Interdisciplinary Research in Chemical Science, and a URC Small Equipment Grant administered by HKU for support of Confocal Raman Microscopy Facilities.

References

1. Furukawa, H.; Cordova, K. E.; O'Keeffe, M.; Yaghi, O. M. The Chemistry and Applications of Metal–Organic Frameworks. *Science* **2013**, *341*, 1230444.
2. Kitagawa, S. Metal–Organic Frameworks (MOFs). *Chem. Soc. Rev.* **2014**, *43*, 5415–5418.
3. Zhou, H. C.; Long, J. R.; Yaghi, O. M. Introduction to Metal–Organic Frameworks. *Chem. Rev.* **2012**, *112*, 673–674.
4. Cao, L.; Lin, Z.; Peng, F.; Wang, W.; Huang, R.; Wang, C.; Yan, J.; Liang, J.; Zhang, Z.; Zhang, T.; Long, L.; Sun, J.; Lin, W. Self-Supporting Metal–Organic Layers as Single-Site Solid Catalysts. *Angew. Chem., Int. Ed.* **2016**, *55*, 4962–4966.
5. Lee, J.; Farha, O. K.; Roberts, J.; Scheidt, K. A.; Nguyen, S. T.; Hupp, J. T. Metal–Organic Framework Materials as Catalysts. *Chem. Soc. Rev.* **2009**, *38*, 1450–1459.
6. Lin, H.; Yang, Y.; Diamond, B. G.; Yan, T.-H.; Bakhmutov, V. I.; Festus, K. W.; Cai, P.; Xiao, Z.; Leng, M.; Afolabi, I.; Day, G. S.; Fang, L.; Hendon, C. H.; Zhou, H. C. Integrating Photoactive Ligands into Crystalline Ultrathin 2D Metal–Organic Framework Nanosheets for Efficient Photoinduced Energy Transfer. *J. Am. Chem. Soc.* **2024**, *146*, 1491–1500.
7. Ma, L.; Falkowski, J. M.; Abney, C.; Lin, W. A Series of Isoreticular Chiral Metal–Organic Frameworks as a Tunable Platform for Asymmetric Catalysis. *Nat. Chem.* **2010**, *2*, 838–846.
8. Zhao, M.; Huang, Y.; Peng, Y.; Huang, Z.; Ma, Q.; Zhang, H. Two-Dimensional Metal–Organic Framework Nanosheets: Synthesis and Applications. *Chem. Soc. Rev.* **2018**, *47*, 6267–6295.
9. Carne, A.; Carbonell, C.; Imaz, I.; Maspoch, D. Nanoscale Metal–Organic Materials. *Chem. Soc. Rev.* **2011**, *40*, 291–305.

10. Cao, L.; Wang, C. Metal–Organic Layers for Electrocatalysis and Photocatalysis. *ACS Cent. Sci.* **2020**, *6*, 2149–2158.
11. Jiang, H. L.; Makal, T. A.; Zhou, H. C. Interpenetration Control in Metal–Organic Frameworks for Functional Applications. *Coord. Chem. Rev.* **2013**, *257*, 2232–2249.
12. Li, Y. Z.; Fu, Z. H.; Xu, G. Metal–Organic Framework Nanosheets: Preparation and Applications. *Coord. Chem. Rev.* **2019**, *388*, 79–106.
13. Wei, Y. S.; Zhang, M.; Zou, R.; Xu, Q. Metal–Organic Framework-Based Catalysts with Single Metal Sites. *Chem. Rev.* **2020**, *120*, 12089–12174.
14. Qiao, G. Y.; Yuan, S.; Pang, J.; Rao, H.; Lollar, C. T.; Dang, D.; Qin, J. S.; Zhou, H. C.; Yu, J. Functionalization of Zirconium-Based Metal–Organic Layers with Tailored Pore Environments for Heterogeneous Catalysis. *Angew. Chem., Int. Ed.* **2020**, *59*, 18224–18228.
15. Mandal, S.; Natarajan, S.; Mani, P.; Pankajakshan, A. Post-Synthetic Modification of Metal–Organic Frameworks toward Applications. *Adv. Funct. Mater.* **2021**, *31*, 2006291.
16. Deria, P.; Mondloch, J. E.; Karagiaridi, O.; Bury, W.; Hupp, J. T.; Farha, O. K. Beyond Post-Synthesis Modification: Evolution of Metal–Organic Frameworks *via* Building Block Replacement. *Chem. Soc. Rev.* **2014**, *43*, 5896–5912.
17. Zheng, H.; Fan, Y.; Song, Y.; Chen, J. S.; You, E.; Labalme, S.; Lin, W. Site Isolation in Metal–Organic Layers Enhances Photoredox Gold Catalysis. *J. Am. Chem. Soc.* **2022**, *144*, 10694–10699.
18. Dhakshinamoorthy, A.; Asiri, A. M.; Garcia, H. 2D Metal–Organic Frameworks as Multifunctional Materials in Heterogeneous Catalysis and Electro/Photocatalysis. *Adv. Mater*. **2019**, *31*, 1900617.
19. Lan, G.; Fan, Y.; Shi, W.; You, E.; Veroneau, S. S.; Lin, W. Biomimetic Active Sites on Monolayered Metal-Organic Frameworks for Artificial Photosynthesis. *Nat. Catal.* **2022**, *5*, 1006–1018.
20. Drake, T.; Ji, P.; Lin, W. Site Isolation in Metal–Organic Frameworks Enables Novel Transition Metal Catalysis. *Acc. Chem. Res.* **2018**, *51*, 2129–2138.
21. Obeso, J. L.; Huxley, M. T.; de Los Reyes, J. A.; Humphrey, S. M.; Ibarra, I. A.; Peralta, R. A. Low–Valent Metals in Metal–Organic Frameworks *via* Post-Synthetic Modification. *Angew. Chem., Int. Ed.* **2023**, *62*, e202309025.
22. Fan, Y.; Blenko, A. L.; Labalme, S.; Lin, W. Metal–Organic Layers with Photosensitizer and Pyridine Pairs Activate Alkyl Halides for Photocatalytic Heck-Type Coupling with Olefins. *J. Am. Chem. Soc.* **2024**, *146*, 7936–7941.
23. Xue, H.; Zhao, Z. H.; Liao, P. Q.; Chen, X. M. "Ship-in-a-Bottle" Integration of Ditin(IV) Sites into a Metal–Organic Framework for Boosting Electroreduction of CO_2 in Acidic Electrolyte. *J. Am. Chem. Soc.* **2023**, *145*, 16978–16982.
24. Qiu, L. Q.; Li, H. R.; He, L. N. Incorporating Catalytic Units into Nanomaterials: Rational Design of Multipurpose Catalysts for CO_2 Valorization. *Acc. Chem. Res.* **2023**, *56*, 2225–2240.
25. Bruns, C. J.; Stoddart, J. F. *The Nature of the Mechanical Bond: From Molecules to Machines*; John Wiley & Sons, Inc: Hoboken, New Jersey, USA, **2016**.
26. Sauvage, J.-P. From Chemical Topology to Molecular Machines (Nobel Lecture). *Angew. Chem., Int. Ed.* **2017**, *56*, 11080–11093.
27. Forgan, R. S.; Sauvage, J. P.; Stoddart, J. F. Chemical Topology: Complex Molecular Knots, Links, and Entanglements. *Chem. Rev.* **2011**, *111*, 5434–5464.
28. Heard, A.W.; Suárez, J. M.; Goldup, S. M. Controlling Catalyst Activity, Chemoselectivity and Stereoselectivity with the Mechanical Bond. *Nat. Rev. Chem.* **2022**, *6*, 182–196.
29. Mo, X.; Deng, Y.; Lai, S. K. M.; Gao, X.; Yu, H. L.; Low, K. H.; Guo, Z.; Wu, H. L.; Au-Yeung, H. Y.; Tse, E. C. Mechanical Interlocking Enhances the Electrocatalytic Oxygen Reduction Activity and Selectivity of Molecular Copper Complexes. *J. Am. Chem. Soc.* **2023**, *145*, 6087–6099.

30. Tang, Y. P.; Luo, Y. E.; Xiang, J. F.; He, Y. M.; Fan, Q. H., Rhodium-Catalyzed ON-OFF Switchable Hydrogenation Using a Molecular Shuttle Based on a [2] Rotaxane with a Phosphine Ligand. *Angew. Chem., Int. Ed.* **2022**, *61*, e202200638.
31. Au-Yeung, H. Y.; Deng, Y. Distinctive Features and Challenges in Catenane Chemistry. *Chem. Sci.* **2022**, *13*, 3315–3334.
32. Zhu, L.; Li, J.; Yang, J.; Au-Yeung, H. Y. Cross Dehydrogenative C–O Coupling Catalysed by a Catenane-Coordinated Copper(I). *Chem. Sci.* **2020**, *11*, 13008–13014.
33. Tang, M. P.; Zhu, L.; Deng, Y.; Shi, Y.; Lai, S. K.-L.; Mo, X.; Pang, X.-Y.; Liu, C.; Jiang, W.; Tse, E. C. M.; Au-Yeung, H. Y. *Angew. Chem. Int. Ed.* **2024**, DOI: 10.1002/anie.202405971.
34. Saura-Sanmartin, A.; Pastor, A.; Martinez-Cuezva, A.; Cutillas-Font, G.; Alajarin, M.; Berna, J. Mechanically Interlocked Molecules in Metal–Organic Frameworks. *Chem. Soc. Rev.* **2022**, *51*, 4949–4976.
35. Ballesteros-Soberanas, J.; Martín, N.; Bacic, M.; Tiburcio, E.; Mon, M.; Hernández-Garrido, J.C.; Marini, C.; Boronat, M.; Ferrando-Soria, J.; Armentano, D.; Pardo, E. A MOF-Supported Pd1–Au1 Dimer Catalyses the Semihydrogenation Reaction of Acetylene in Ethylene with a Nearly Barrierless Activation Energy. *Nat. Catal*. **2024**, *7*, 452–463.
36. Chen, Y.; Jiménez-Ángeles, F.; Qiao, B.; Krzyaniak, M. D.; Sha, F.; Kato, S.; Gong, X.; Buru, C. T.; Chen, Z.; Zhang, X.; Gianneschi, N. C.; Wasielewski, M. R.; Olvera de la Cruz, M.; Farha, O. K. Insights into the Enhanced Catalytic Activity of Cytochrome c When Encapsulated in a Metal–Organic Framework. *J. Am. Chem. Soc.* **2020**, *142*, 18576–18582.
37. Rodríguez-Rubio, A.; Savoini, A.; Modicom, F.; Butler, P.; Goldup, S. M. A Co-Conformationally "Topologically" Chiral Catenane. *J. Am. Chem. Soc.* **2022**, *144*, 11927–11932.
38. Gallagher, J. M.; Roberts, B. M. W.; Borsley, S.; Leigh, D. A. Conformational Selection Accelerates Catalysis by an Organocatalytic Molecular Motor. *Chem* **2023**, *10*, 855–866.
39. Feng, L.; Astumian, R. D.; Stoddart, J. F. Controlling Dynamics in Extended Molecular Frameworks. *Nat. Rev. Chem.* **2022**, *6*, 705–725.
40. Wilson, B. H.; Loeb, S. J. Integrating the Mechanical Bond into Metal–Organic Frameworks, *Chem* **2020**, *6*, 1604–1612.
41. Hu, Z.; Mahdi, E. M.; Peng, Y.; Qian, Y.; Zhang, B.; Yan, N.; Yuan, D.; Tan, J. C.; Zhao, D. Kinetically Controlled Synthesis of Two-Dimensional Zr/Hf Metal–Organic Framework Nanosheets via a Modulated Hydrothermal Approach. *J. Mater. Chem. A* **2017**, *5*, 8954–8963.
42. Tao, Z. R.; Wu, J. X.; Zhao, Y. J.; Xu, M.; Tang, W. Q.; Zhang, Q. H.; Gu, L.; Liu, D. H.; Gu, Z. Y. Untwisted Restacking of Two-Dimensional Metal–Organic Framework Nanosheets for Highly Selective Isomer Separations. *Nat. Commun.* **2019**, *10*, 2911.
43. Wang, Y.; Feng, L.; Pang, J.; Li, J.; Huang, N.; Day, G. S.; Cheng, L.; Drake, H. F.; Wang, Y.; Lollar, C.; Qin, J.; Gu, Z.; Lu, T.; Yuan, S.; Zhou, H. C. Photosensitizer-Anchored 2D MOF Nanosheets as Highly Stable and Accessible Catalysts toward Artemisinin Production. *Adv. Sci.* **2019**, *6*, 1802059.
44. Feng, L.; Qiu, Y.; Guo, Q.-H.; Chen, Z.; Seale, J. S. W.; He, K.; Wu, H.; Feng, Y.; Farha, O. K.; Astumian, R. D.; Stoddart, J. F. Active Mechanisorption Driven by Pumping Cassettes. *Science* **2021**, *374*, 1215–1221.
45. Sauvage, J. P.; Weiss, J. Synthesis of Biscopper(I) [3]-Catenates: Multiring Interlocked Coordinating Systems. *J. Am. Chem. Soc.* **1985**, *107*, 6108-6110.
46. Shimoni, R.; Shi, Z.; Binyamin, S.; Yang, Y.; Liberman, I.; Ifraemov, R.; Mukhopadhyay, S.; Zhang, L.; Hod, I. Electrostatic Secondary-Sphere Interactions That Facilitate Rapid and Selective Electrocatalytic CO_2 Reduction in a Fe-Porphyrin-Based Metal–Organic Framework. *Angew. Chem., Int. Ed.* **2022**, *61*, e202206085.

47. Zhao, M. T.; Chen, J. Z.; Chen, B.; Zhang, X.; Shi, Z. Y.; Liu, Z. Q.; Ma, Q. L.; Peng, Y. W.; Tan, C. L.; Wu, X. J.; Zhang, H. Selective Epitaxial Growth of Oriented Hierarchical Metal–Organic Framework Heterostructures. *J. Am. Chem. Soc.* **2020**, *142*, 8953–8961.
48. Kumar, G. S.; Maheswari, C. U.; Kumar, R. A.; Kantam, M. L.; Reddy, K. R. Copper-Catalyzed Oxidative C-O Coupling by Direct C-H Bond Activation of Formamides: Synthesis of Enol Carbamates and 2-Carbonyl-Substituted Phenol Carbamates. *Angew. Chem., Int. Ed.* **2011**, *50*, 11748–11751.
49. Li, C. J. Cross-Dehydrogenative Coupling (CDC): Exploring C−C Bond Formations Beyond Functional Group Transformations. *Acc. Chem. Res.* **2009**, *42*, 335–344.
50. Li, C. J.; Li, Z. Green Chemistry: The Development of Cross–Dehydrogenative Coupling (CDC) for Chemical Synthesis. *Pure Appl. Chem.* **2006**, *78*, 935–945.
51. Scheuermann, C. J. Beyond Traditional Cross Couplings: The Scope of the Cross Dehydrogenative Coupling Reaction. *Chem.-Asian J.* **2010**, *5*, 436–451.
52. Miao, C. B.; Wang, Y. H.; Xing, M. L.; Lu, X. W.; Sun, X. Q.; Yang, H. T. I_2-Catalyzed Direct α-Hydroxylation of β-Dicarbonyl Compounds with Atmospheric Oxygen under Photoirradiation. *J. Org. Chem.* **2013**, *78*, 11584–11589.